



HAL
open science

Pairwise hydrodynamic interactions and diffusion in a vesicle suspension

Pierre-Yves Gires, Aparna Srivastav, Chaouqi Misbah, Thomas Podgorski,
Gwennou Coupier

► **To cite this version:**

Pierre-Yves Gires, Aparna Srivastav, Chaouqi Misbah, Thomas Podgorski, Gwennou Coupier. Pairwise hydrodynamic interactions and diffusion in a vesicle suspension. *Physics of Fluids*, 2014, 26, pp.013304. 10.1063/1.4861900 . hal-00932398

HAL Id: hal-00932398

<https://hal.science/hal-00932398>

Submitted on 17 Jan 2014

HAL is a multi-disciplinary open access archive for the deposit and dissemination of scientific research documents, whether they are published or not. The documents may come from teaching and research institutions in France or abroad, or from public or private research centers.

L'archive ouverte pluridisciplinaire **HAL**, est destinée au dépôt et à la diffusion de documents scientifiques de niveau recherche, publiés ou non, émanant des établissements d'enseignement et de recherche français ou étrangers, des laboratoires publics ou privés.

Pairwise hydrodynamic interactions and diffusion in a vesicle suspension

Pierre-Yves Gires,^{1, a)} Aparna Srivastav,^{1, b)} Chaouqi Misbah,¹ Thomas Podgorski,¹ and
Gwennou Coupier^{1, c)}

*Laboratoire Interdisciplinaire de Physique, CNRS - UMR 5588,
Université Grenoble I, B.P. 87, 38402 St Martin d'Hères Cedex,
France*

(Dated: 30 December 2013)

The hydrodynamic interaction of two deformable vesicles in shear flow induces a net displacement, in most cases an increase of their distance in the transverse direction. The statistical average of these interactions leads to shear-induced diffusion in the suspension, both at the level of individual particles which experience a random walk made of successive interactions, and at the level of suspension where a non-linear down-gradient diffusion takes place, an important ingredient in the structuring of suspension flows. We make an experimental and computational study of the interaction of a pair of lipid vesicles in shear flow by varying physical parameters, and investigate the decay of the net lateral displacement with the distance between the streamlines on which the vesicles are initially located. This decay and its dependency upon vesicle properties can be accounted for by a simple model based on the well established law for the lateral drift of a vesicle in the vicinity of a wall. In the semi-dilute regime, a determination of self-diffusion coefficients is presented.

PACS numbers: 82.70.Uv, 83.80.Lz, 83.50.Ha

^{a)}Now at Laboratoire de Biomécanique et de Bioingénierie, UMR CNRS 7338, Université de Technologie de Compiègne, France.

^{b)}Now at Zentralinstitut für Medizintechnik, Technische Universität München, Germany; both first authors equally contributed to the production of the data presented in this paper. P.-Y. G. produced the theoretical and computational results and A. S. performed the experiments.

^{c)}Electronic mail: gwennou.coupier@ujf-grenoble.fr

I. INTRODUCTION

Liquid suspensions of deformable particles are the focus of permanent interest due to their ubiquity in life science and applications, from emulsions to blood, a dense suspension of red blood cells. It is well known since Batchelor^{1,2} that the viscosity of a semi-dilute suspension of rigid spheres departs from the classic linear Einstein law of viscosity for volume fractions of particles above a few percents, due to the additional dissipation induced by hydrodynamic interactions between particles.

In addition to their influence on the effective viscosity at significant volume fractions, these hydrodynamic interactions (which are sometimes called binary collisions in the literature, although still mediated by hydrodynamics) can lead to irreversible perturbations of the particle trajectories which result in an effective random walk of individual particles in the suspension. This shear-induced diffusion has two main consequences: enhanced mixing and transport even at low Reynolds number³⁻⁸, and a modification of the structure of suspensions via diffusion along gradients of concentration of the particles⁹⁻¹².

In shear flow, two identical particles located on different streamlines and moving towards each other will generally experience irreversible drift in the shear and vorticity directions after they have interacted. However, for smooth rigid spherical particles in a dilute regime dominated by pairwise interactions, the cross-stream lateral displacement is expected to be negligible at low Reynolds number since trajectories must be symmetric due to the flow-reversal symmetry of the Stokes equation¹³ and the symmetry of the geometrical configuration. Symmetry breaking can be obtained by considering rough particles^{14,15} or deformable two-fluid systems such as bubbles¹⁶ or drops¹⁷⁻²⁰. More recently, systems made of closed membranes have been investigated numerically or experimentally. Hydrodynamic interaction between elastic capsules were studied numerically in several papers²¹⁻²⁴. During the interaction, net displacement of the capsules can be coupled with wrinkling or buckling of the membranes, whose tension strongly increases during interaction.

The dynamics and rheology of suspensions of lipid vesicles have recently been the focus of several studies, due to their relevance to the understanding of blood flows, considering giant vesicles as models of red blood cells, and the challenging theoretical questions they pose as a consequence of their rich microscopic dynamics. Vesicles are closed lipid bilayers with mechanical properties similar to those of living cells. A key property is the membrane

Set	Solution	η (mPa.s)	$\lambda = \frac{\eta_I}{\eta_E}$
1	(I) 300mM sucrose in (20% glycerol + 80% water w/w)	2.2	1.0
	(E) 370mM glucose in (20% glycerol + 80% water w/w)	2.2	
2	(I) 100mM sucrose in water + 3.3% dextran w/w	4.2	3.8
	(E) 115mM glucose in water	1.1	
3	(I) 300mM sucrose in water	1.1	0.28
	(E) 316mM glucose in water + 3% dextran w/w	4.0	

TABLE I. Sets of internal (I) and external (E) solutions considered in the experiments. Viscosities η are measured at $T = 23^\circ$ C.

inextensibility, which leads to local area conservation, while volume conservation is generally obtained once osmotic equilibrium is reached. The vesicles mechanical response, as well as their shapes²⁵, are governed by a bending energy of order a few kT , where k is Boltzmann's constant and T the temperature. These particular properties, especially the non-linearities due to the constraint of local area conservation, are responsible for the various dynamics of single vesicles in shear flow^{26–28}. The phase diagram of microscopic dynamics has a signature on the rheology of vesicle suspensions²⁹, but there is still disagreement, especially in the semi-dilute regime where two experimental studies show contradictory results^{30,31}. In an effort to resolve this contradiction, Kantsler et al.³⁰ and Levant et al.³² have investigated the influence of interactions on fluctuations and correlations of the inclination angles of interacting vesicles and suggest that they may be responsible for discrepancies between theories in the dilute regime and experimental measurements of the effective viscosity, which are often made in a semi-dilute regime for sensitivity reasons. On the analytical side, the trajectories of interacting vesicles have been recently studied in the limit where they are initially very distant from each other³³. This study has been later on refined in the case of vesicles located in the same shear plane³⁴. Very recently, such trajectories have been calculated numerically by Zhao and Shaqfeh³⁵. They also calculated the rheology of a semi-dilute suspension and found good agreement with the experiments by Vitkova et al.³¹, a strong indication that, in that concentration regime, interactions between vesicles cannot explain the contradiction between the latter experiments and the one by Kantsler et al.³⁰

Along with their influence on rheology, hydrodynamic interactions significantly affect the

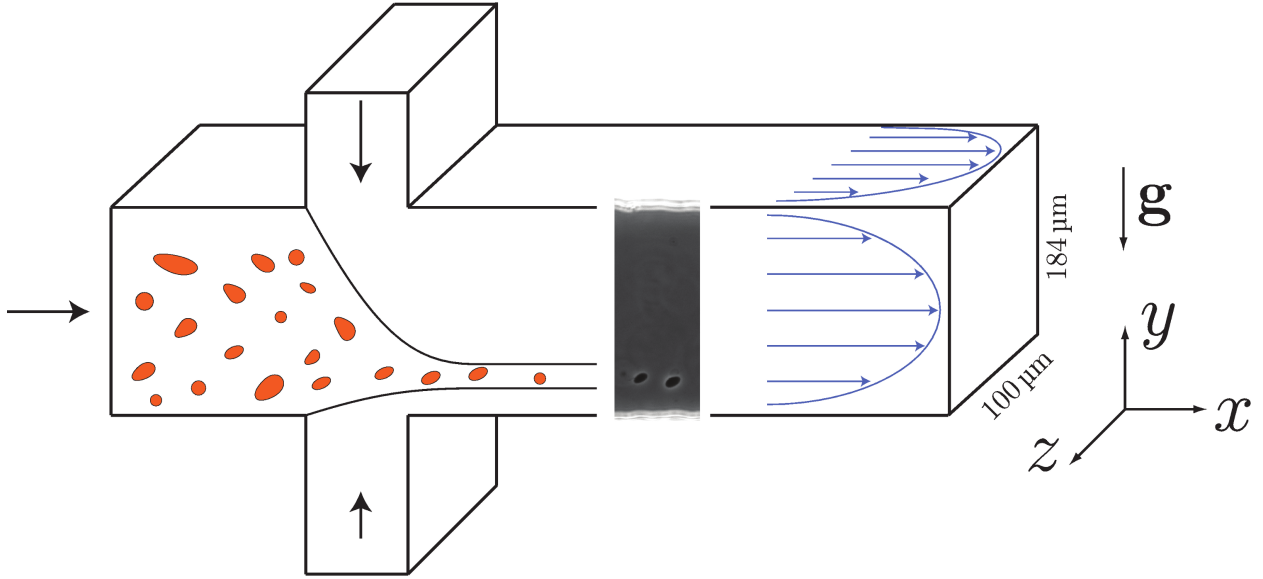


FIG. 1. Sketch of the experiment.

structure of suspensions, especially in confined flows where a balance between migration away from walls and shear-induced diffusion due to repulsive interactions leads to the formation of a non-homogeneous distribution of vesicles¹¹. During heterogeneous interactions of vesicles or capsules with different mechanical or geometrical characteristics, asymmetric displacements take place, which leads to segregation or margination^{7,11,36–38}, a phenomenon also observed in blood flows^{39–42}.

In this paper, we report on our experimental and numerical investigation of the interaction of two identical vesicles in shear flow, with a focus on the net lateral displacement as a function of initial configuration and vesicle properties.

With a good agreement between experiments and simulations, the amplitude of the lateral displacement is found to be weakly dependent on vesicle deflation and viscosity ratio, at least in the tank-treading regime to which we restrict our study. Thanks to the simulations, we also discuss to which extent the discrepancies between the ideal case of two identical and neutrally buoyant vesicles, placed in the shear plane of an infinite simple shear flow, and the realistic case of channel flow, influence the final result.

Finally, from the numerical results, an evaluation of the self-diffusion coefficient, obtained by averaging displacements over all initial configurations, is proposed and compared to the recent results of Zhao and Shaqfeh³⁵.

II. EXPERIMENTAL SET-UP

Fluid vesicles are prepared by following the electroformation method⁴³, which produces vesicles of various size and deflation (that is, the surface to volume ratio). They are made of a dioleoylphosphatidylcholine (DOPC) lipid bilayer. We consider three sets of outer and inner solutions in order to vary the viscosity ratio λ between the inner and the outer fluids (see table I). The different additives (sugars and dextran) used for inner and outer solutions provide an optical index contrast which is convenient for phase contrast microscopy.

We wish to observe interactions in simple shear flow between vesicles located in the same xy plane, where x is the flow direction and y the shear direction. To that end, the vesicle suspension is injected in a standard polydimethylsiloxane (PDMS) microfluidic device. The observation channel is $184\ \mu\text{m}$ wide (y direction) and $100\ \mu\text{m}$ deep (z direction). The imposed flow is along the x axis (see Fig. 1). Before the observation section, vesicles flow in a channel of several centimeters long, so that centering in the z direction is generally rather well achieved⁴⁴, as confirmed by the location of all vesicles within a focal plane of thickness of order $5\ \mu\text{m}$. The interacting vesicles were followed manually translating the stage. The observation window is $477 \times 358\ \mu\text{m}^2$, with a resolution of $0.47\ \mu\text{m}/\text{pixel}$. The use of a channel flow, rather than a four-roll mill device^{30,32}, allows to measure the final lateral displacement due to the interaction, a key parameter in the discussion of diffusion phenomena.

As measurable interactions only occur when vesicles have initial y separation not larger than 2 radii, it appeared necessary to favor such an initial condition by adding a flow focusing device at the entrance of the observation channel. Two lateral inlets were then added, where vesicle-free fluid was injected in order to focus the suspension in a narrow area. This area is located at around one fourth of the total width of the channel, that is, far from the wall and far from the center, where the flow can be considered as a simple shear flow, in a first approximation to be discussed later. Vesicles stay at this favorable position thanks to the balance between lift forces⁴⁴⁻⁴⁶ and gravity. In addition, dilution by the lateral inlets decreases the probability of perturbation of the interaction trajectories by other vesicles.

In the observation window, at most 3 or 4 vesicles (including the two studied vesicles) are present at the same time. In the selected interaction sequences, the additional vesicles of non negligible size are always at a distance from the pair larger than 5 radii and are located almost on the same streamlines, so that they will not come close to the pair within

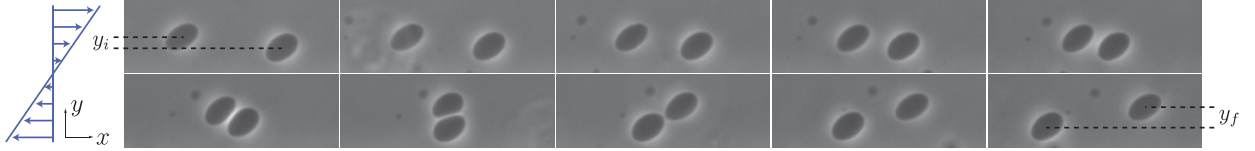


FIG. 2. Time sequence of an experimental interaction (left to right and top to bottom). Bottom vesicle: $R_1 = 9.3 \mu\text{m}$, $\nu_{a1} = 0.94$. Top vesicle: $R_2 = 9.2 \mu\text{m}$, $\nu_{a2} = 0.92$. Total sequence length is about 5 s.

the duration of the studied interaction process. As in Fig. 2, very small vesicles may come closer, but the induced perturbation is expected to be negligible: from an asymptotic approach³³, we can expect the velocity perturbations induced by a vesicle 4 times smaller than the studied ones to be smaller than the one coming from the interacting vesicles by a factor $(\frac{1}{4})^2 = 0.06$.

Once an appropriate pair of vesicles is chosen, the vesicles are followed along their trajectories and the (x, y) coordinates of the vector linking their geometrical centers are determined, as well as their shapes. We denote by (x_i, y_i) the initial position and by (x_f, y_f) the final one. By convention, $x_i < 0$ and $y_i > 0$. An example of selected snapshots taken along a trajectory is shown in Fig. 2. As we only have access to their two-dimensional cross-section in the xy plane, we characterize the 2D shapes by the effective radius R_i , $i = 1, 2$, defined by $R_i = \mathcal{P}_i / (2\pi)$, where \mathcal{P}_i is the cross-section perimeter, and by a reduced area $\nu_{ai} = \mathcal{A}_i / (\pi R_i^2) \leq 1$, where \mathcal{A}_i is the cross-sectional area. These two parameters are evaluated before the vesicles strongly interact, at which point out-of-plane deformations occur.

In this study, we focus on pairs of vesicles of similar size and deflation (within maximal variations of 10 percent for the radii and 5 percent for the reduced area). We denote by R_0 and ν_a the arithmetic averages of the radii and reduced areas of the two interacting vesicles. R_0 lies between 5 and 19 μm , and ν_a between 0.73 and 1. The flow velocity is set so that the capillary number lies typically between 10 and 100. This capillary number $Ca = \eta \dot{\gamma} a^3 / \kappa$ qualitatively represents the ratio between the magnitude of the liquid viscous stresses exerted on a membrane, and its resisting bending stresses, controlled by bending rigidity κ . $\dot{\gamma}$ is the shear rate and η the suspending fluid viscosity. a is the effective radius of the vesicle, defined from its volume V by $V = 4\pi a^3 / 3$. Note that, due to vesicle volume

conservation, this 3D effective radius is constant and characteristic of the considered vesicle, while the observed 2D radius R_0 depends on the applied flow. As a can only be roughly estimated in the experiments, we only have access to estimated values for Ca .

From the obtained trajectories, we extract the main information, that is the lateral displacement $\Delta_y = y_f - y_i$ as a function of initial lateral separation y_i . Both distances are rescaled by R_0 . Several initial positions y_i are scanned either by considering different pairs of vesicles, or by making a given pair going back and forth thanks to flow reversal.

III. EXPERIMENTAL RESULTS

We first focus on vesicles with no viscosity contrast. Results for Δ_y/R_0 as a function of y_i/R_0 are shown in Fig. 3. Initial and final y positions are measured by averaging over several positions long before and after interaction. Error bars are associated to the fluctuations in these y positions due to the presence of other small vesicles or flow variations due to channel roughness. Such events are likely to occur because of the large ratio between the relative velocity along the x axis between the considered vesicles and the other vesicles or the wall, and the velocity along the y axis. The studied pairs are split into two subpopulations according to their reduced areas. Vesicles with $\nu_a > 0.99$ undergo negligible deviations which are not measurable within experimental errors. This result is expected for spherical particles and allows to check that no uncontrolled drift alters the experimental results. All other pairs of vesicles yield comparable deviations whatever the reduced area in the range $0.82 - 0.98$. Data scattering can be due to variations in reduced areas (including within a pair), sizes, capillary numbers, but also to non complete collocation in the same xy plane. In addition, displacements might be affected by the flow perturbation induced by the walls, which depends on the lateral position of the vesicles, a parameter that varies from one pair to another.

Lateral deviation is a decreasing function of initial lateral separation, and becomes negligible for initial lateral separations greater than one diameter. An empirical estimate for this deviation can be obtained by considering that, in the reference frame of the bottom vesicle, the displacement of the top vesicle is due to the interaction with a wall of finite extent in the x direction, whose role is played by the bottom vesicle. The lift velocity of a vesicle in a simple shear flow and at a distance y from a wall was experimentally shown⁴⁶ to agree with

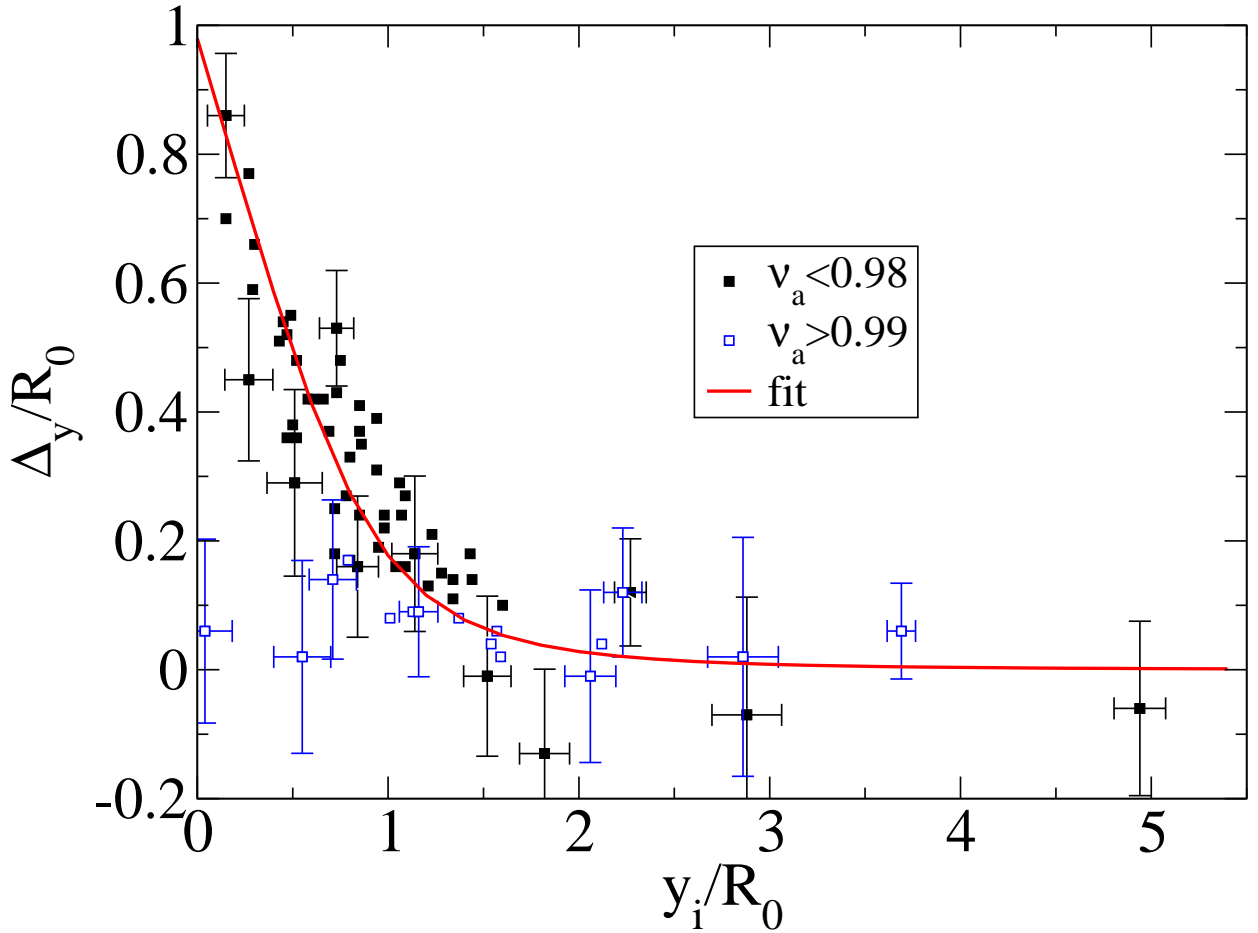


FIG. 3. Experimental lateral displacements Δ_y/R_0 as a function of y_i/R_0 for vesicles with no viscosity contrast ($\lambda = 1$). Empty symbols correspond to vesicles with reduced area $\nu_a > 0.99$, while vesicles of reduced area between 0.82 and 0.98 are represented by full symbols. Full line shows fit to this latter data set with empirical law given by Eq. 1 with fit parameter $\xi = 0.92$. Error bars correspond to a spatial uncertainty of $1 \mu\text{m}$. Only part of them are presented for clarity.

the scaling law $\dot{y} = U\dot{\gamma}R_0^3/y^2$ suggested or confirmed by several theoretical works^{34,47-49}, where U is a dimensionless parameter that depends on viscosity ratio and reduced volume. The reduced volume ν is defined as the ratio between the vesicle volume and the volume of the sphere having the same area; due to volume conservation and membrane incompressibility, this is a constant parameter that characterizes the deflation of the vesicle. The top vesicle flows with relative velocity $\dot{x} = \dot{\gamma}y$, so that $dy/dx = UR_0^3/y^3$. Interaction takes place on a finite distance of order $2R_0$. Integrating the latter equation on this distance for x and between y_i and y_f for y , one finally finds

$$\Delta_y/R_0 = (y_i^4/R_0^4 + \xi)^{1/4} - y_i/R_0, \quad (1)$$

where $\xi = 8U$ contains the interaction details. $\xi^{1/4}$ is the maximal displacement, obtained for $y_i \rightarrow 0$. Taking an estimate of U from Olla's work⁴⁷, we have for a prolate ellipsoid with $\nu_a = 0.9$, $\xi^{1/4} \sim 1.2$, which is close to the maximal displacement seen in Fig. 3, where a full fit of the whole data set with Eq. 1 yields $\xi = 0.92$. Note that this is a single parameter fit, so that the distance at which interaction becomes negligible is fully determined by the maximal deviation obtained for quasi-aligned vesicles. In particular, vesicles initially distant by one diameter in the y direction will deviate only by $(16 + \xi)^{1/4} - 2 \lesssim 2\%$ from their initial trajectories.

From this law, we can estimate how the final displacement should vary with reduced volume. Following for instance the recent study by Farutin and Misbah³⁴, U scales as $(1 - \nu)^{\frac{1}{2}}$, so that the maximal displacement scales as $(1 - \nu)^{\frac{1}{8}}$. This sharp increase around $\nu = 1$ explains the strong difference between the quasi-spherical vesicles ($\nu_a > 0.99$) and the more deflated ones ($\nu_a < 0.98$) seen on Fig. 3. On the other hand, from Olla's results⁴⁷, U is multiplied by a factor 2.7 between prolate vesicles of reduced areas 0.98 and 0.82, respectively. The maximum displacement for vanishing y_i should then be multiplied by $2.7^{1/4} \simeq 1.3$. Such a tiny variation is within the scattering and error of experimental data.

Similarly, when the viscosity ratio is varied, no significant displacement variation is observed, as shown in Fig. 4. Once again, this is consistent with our empirical law, since from Olla's results again, for $\nu_a = 0.9$, $U^{1/4}$ decreases only by 2% between vesicles of viscosity ratio 0.28 and 1, and by 12% between vesicles of viscosity ratio 1 and 3.8. According to Zhao and Shaqfeh³⁵, the maximum displacement drops by about 30% between viscosity ratio 1 and 7.

In the next section, we address the same questions with full 3D numerical simulations restricted to the case $\lambda = 1$, following our discussion on the weak influence of the viscosity ratio in the previous section. We then confront the numerical results with the experimental ones.

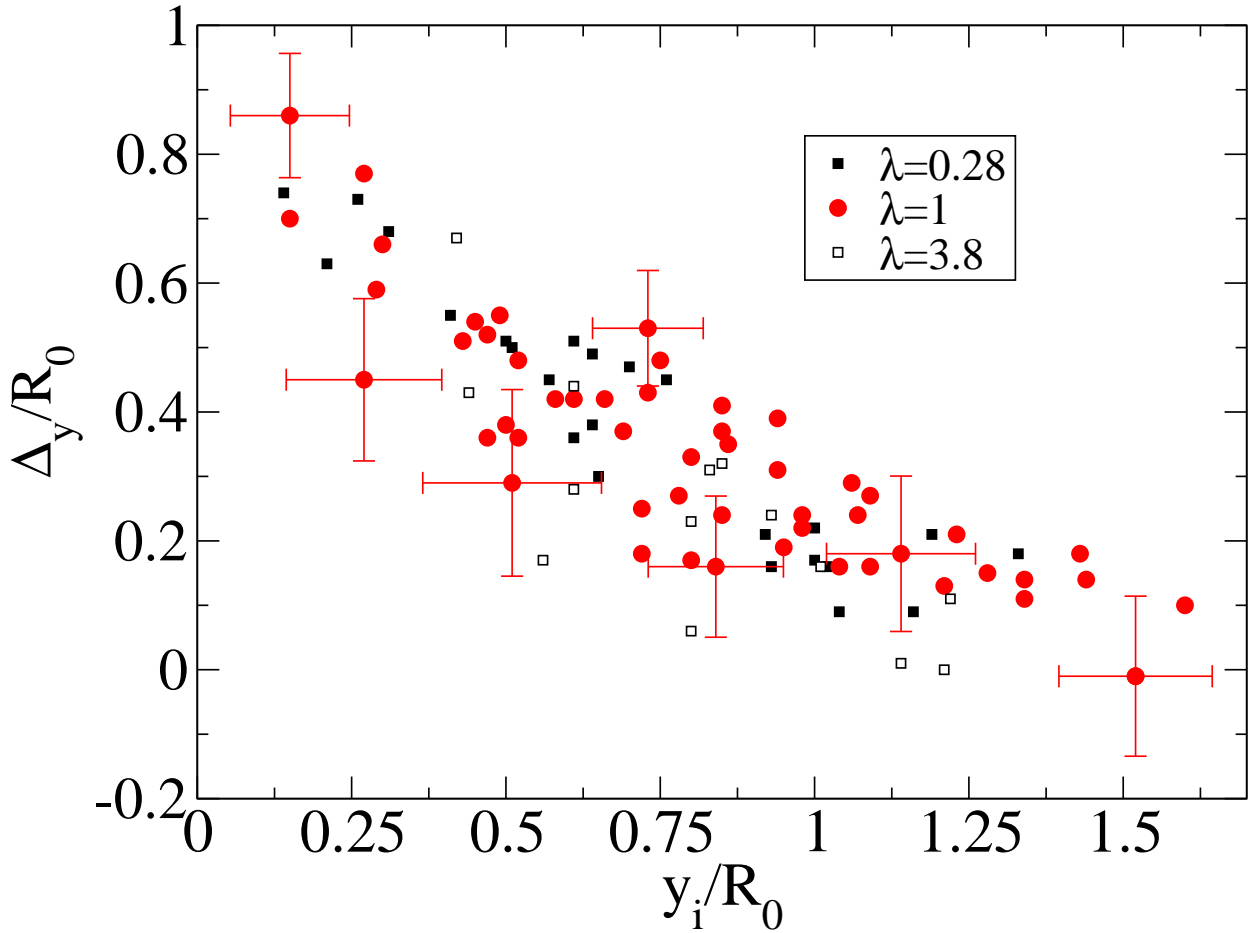


FIG. 4. Experimental lateral displacements Δ_y/R_0 as a function of y_i/R_0 for vesicles with different viscosity ratios; $\lambda = 0.28$: $\nu_a \in [0.73; 0.98]$; $\lambda = 1$: $\nu_a \in [0.82; 0.98]$; $\lambda = 3.8$: $\nu_a \in [0.77; 0.98]$. Error bars correspond to a spatial uncertainty of $1 \mu\text{m}$. Only part of them are presented for clarity.

IV. MODEL AND NUMERICAL METHOD

A. Liquid and membrane

In this section we outline the model and numerical method. The internal and external liquids are modeled as incompressible, homogeneous, Newtonian fluids. We restrict our study to the case where their densities, as well as their viscosities, are equal. Both liquids flow in the creeping regime.

The membranes are modeled by two dimensional surfaces. As for the liquids, their inertia is negligible. Their areas stay locally constant. They resist bending with an energy E_b , given by⁵⁰

$$E_b = \int_A \frac{\kappa}{2} (2H)^2 dA, \quad (2)$$

where A is the membrane surface, κ the bending rigidity, and H the mean curvature. The sign convention for the curvatures is taken so that the mean curvature of a sphere is negative.

The resulting surface force density that the membrane exerts on the fluids is

$$\mathbf{f} = -\{\kappa[2H(2H^2 - 2K) + 2\Delta_s H] - 2\zeta H\}\mathbf{n} + \nabla_s \zeta,$$

where \mathbf{n} is the unit normal vector pointing outward, K the Gaussian curvature, and ζ a Lagrange multiplier that enters the total energy, obtained by adding to (2) $\int_A \zeta dA$. It ensures local membrane incompressibility and satisfies:

$$\nabla_s \cdot \mathbf{v} = 0, \quad (3)$$

where ∇_s is the surface gradient operator and \mathbf{v} is the membrane velocity.

Note that we don't include in our model any other small range interaction than the hydrodynamic forces within the lubricating film, described as squeezed between athermal membranes. As a first approximation, we considered that these stresses grow fast enough so that the minimal distance between the membranes, that we denote d , remains higher than a typical distance under which other type of interactions become significant. The first one that would appear is linked to the inhibition of thermal fluctuations⁵¹, which leads to an entropic repulsion pressure. It is of order $0.2(k_B T)^2 / (\kappa d^3)$. It would balance the imposed pressure, estimated as $\eta \dot{\gamma}$, that tends to push the two vesicles towards each other, if

$$d \sim \left(\frac{0.2(k_B T)^2}{\kappa \eta \dot{\gamma}} \right)^{1/3}. \quad (4)$$

Using the typical value $\kappa \sim 20k_B T$, for the smallest shear rate in our experiments $1s^{-1}$, one finds that d reaches values in the range of 100nm. We checked that, in the trajectories we investigated, d remains higher than the previous estimate. The facts that the entropic force is repulsive, and that, on the contrary to some rigid particles, there are no heterogeneities on the phospholipid membranes that can facilitate the drainage of the lubricating film, support even more our approximation.

B. Boundary conditions

The membranes are supposed to be at osmotic equilibrium and are modeled as impermeable. Together with the no slip boundary condition, this leads to an advection of the membranes with the local velocity of the flow.

A force balance on the membrane yields

$$\mathbf{f} = -(\sigma^+ - \sigma^-) \cdot \mathbf{n}, \quad (5)$$

where σ is the liquid stress tensor with a + or - superscript respectively for the external and internal fluids, defined as $\sigma = -p\mathbb{1} + \eta(\nabla\mathbf{v} + (\nabla\mathbf{v})^t)$. Far from the vesicles, the imposed simple shear flow $\mathbf{v}^\infty = \dot{\gamma}y\mathbf{e}_x$ is recovered.

We denote by $\mathbf{R}_{12} = (x, y, z)$ the vector linking the centers of mass C_i of the two vesicles. We shall study the evolution of (y, z) as a function of x , that is, the trajectory of vesicle 2 in the frame centered on vesicle 1. Different initial positions (y_i, z_i) will be scanned, with initial longitudinal distance x_i much larger than the vesicles radii. A sketch of the initial state of the system is presented in Fig. 5.

C. Numerical method

The full set of equations in the Stokes regime can be converted into a boundary integral formulation⁵². The integral equation (recalled below) is solved numerically in three dimensions following the work by Biben *et al.*²⁸. The new elements of the present study are the extensions to two vesicles and, in a second time, to the presence of a wall that turns out to be a relevant ingredient when confronting the numerical results with the experimental one. We shall first study the situation without wall, which is the main goal of the paper.

The integral equation provides the expression of the membrane velocities as a function of boundary integrals and reads

$$v_\alpha(\mathbf{r}) = v_\alpha^\infty(\mathbf{r}) + \int_{\partial\Omega} G_{\alpha\beta}(\mathbf{r}, \mathbf{r}') f_\beta(\mathbf{r}') dA', \quad (6)$$

where \mathbf{r} is the position vector of a membrane point, $\partial\Omega$ the boundaries present in the system under consideration, which are in the present case the two vesicle membranes, and $G(\mathbf{r}, \mathbf{r}')$ the Green's function of an incompressible fluid following Stokes equation. As we

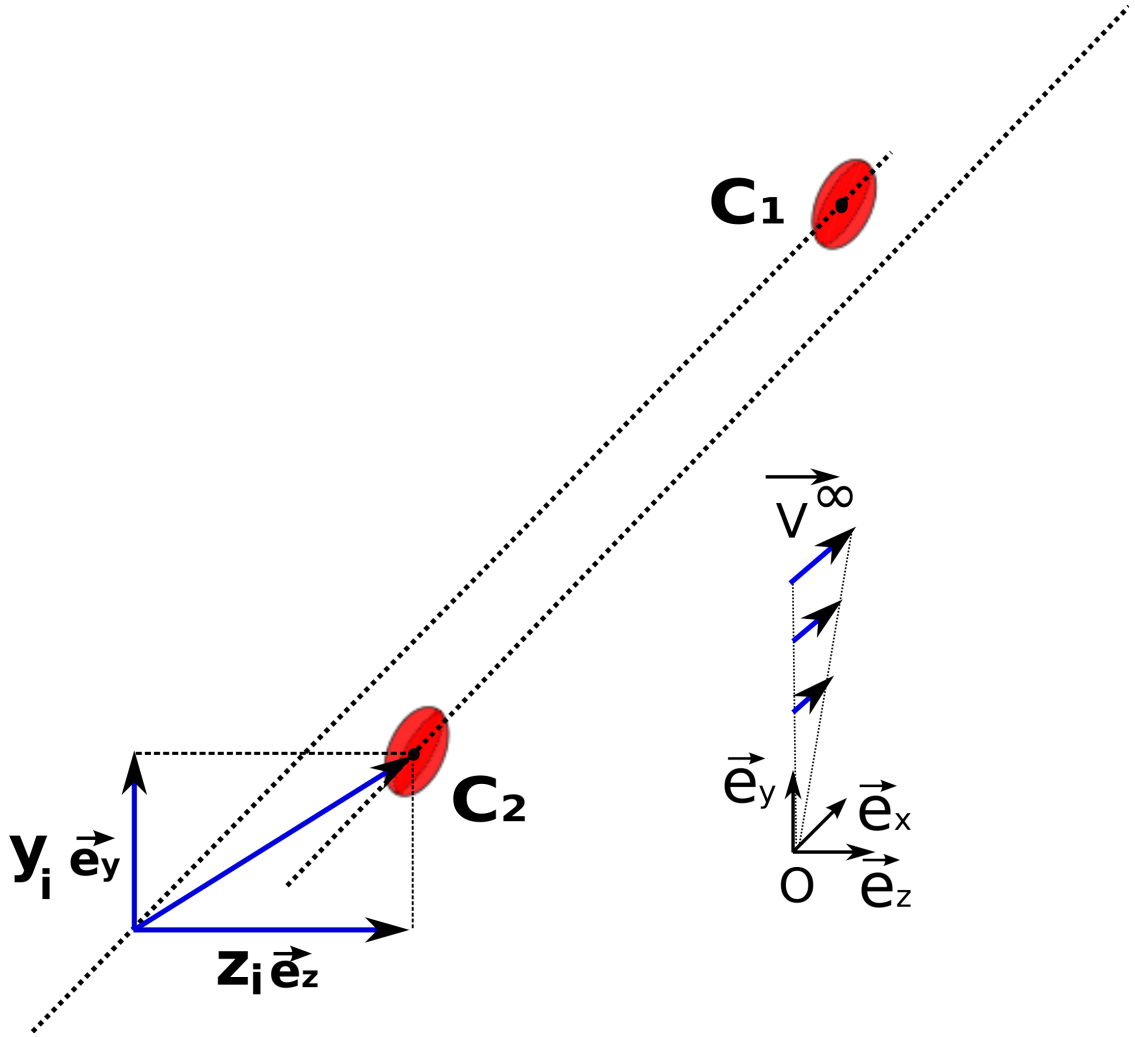


FIG. 5. A schematic view of the initial state of the system

consider an unbounded domain, an appropriate choice is the Green's function associated to a point force in an infinite liquid, such that $G_{\alpha\beta}(\mathbf{r}, \mathbf{r}') = G_{\alpha\beta}^{\infty}(\mathbf{r} - \mathbf{r}')$, where⁵²

$$G_{\alpha\beta}^{\infty}(\mathbf{r}) = \frac{1}{8\pi\eta} \left(\frac{\delta_{\alpha\beta}}{r} + \frac{r_{\alpha}r_{\beta}}{r^3} \right). \quad (7)$$

For most simulations, the vesicles are meshed by 642 vertices, and the time step is $10^{-4}\eta a^3/\kappa$. We checked that for a typical trajectory $((y_i, z_i) = (0.5, 0))$, results were relatively independent from a reduction of the mesh size and time step: increasing the number of vertices to 2562 and reducing the time step by a factor 2 led to relative changes in the transverse migration of 0.3%. A challenge is to achieve an evolution of the membrane shapes ensuring a local conservation of the area. We present in appendix A details showing that

our study conserves the area with a good approximation. The simulations start with both vesicles having the steady inclination angle of an isolated vesicle in shear flow, obtained from a preliminary simulation.

V. NUMERICAL RESULTS

A. Identical vesicles in the same shear plane

We start with the case of identical vesicles, with the typical parameters ($\lambda = 1, \nu = 0.95$), in the same shear plane of an infinite simple shear flow. The capillary number is taken in the set $\{10, 50, 100\}$, so that the whole range of possible experimental values is covered. We plot in Fig. 6 the interaction curve $\Delta_y(y_i)$ (that is the difference between the final and initial y -positions), with initial and final distances corresponding to $x_i = -10a$ and $x_f = 10a$.

For all values of Ca , we recover the decrease of Δ_y/R_0 from around 1 to zero. All deviations become smaller than 0.1 for $y_i/R_0 > 2.5$. There is a good agreement with the simple model based on the law for the lift of a vesicle near a wall, that was presented in the preceding section. It thus validates this model as a convenient tool to anticipate the dependency of the lift with the mechanical properties of the vesicles. Note however that, since the shape in Olla's model is prescribed, no dependency on Ca can arise from it.

Overall, considering that there are no fitting parameters (but some experimental uncertainty on C_a), the agreement is rather satisfactory. However, the experiments lead to smaller displacements, as the numerical curve passes through the error bars of only about 30% of the experimental points. This discrepancy may be explained by differences between the experimental configuration and the ideal unbounded simple shear flow on three aspects. First, the suspension is slightly polydisperse, both in shape and size. Second, the centering in the z direction might not be perfect. Indeed, the depth of focus of the microscope is about $5\mu\text{m}$, which allows z_i to differ from 0 by amounts up to $R_0/2$. Third, the balance between wall-induced lift forces and sedimentation in the y direction is perturbed during the interaction, and may also not be fully reached before interaction starts, because of preceding interactions. All those effects could be non negligible. We use the numerical model to study their relative importance.

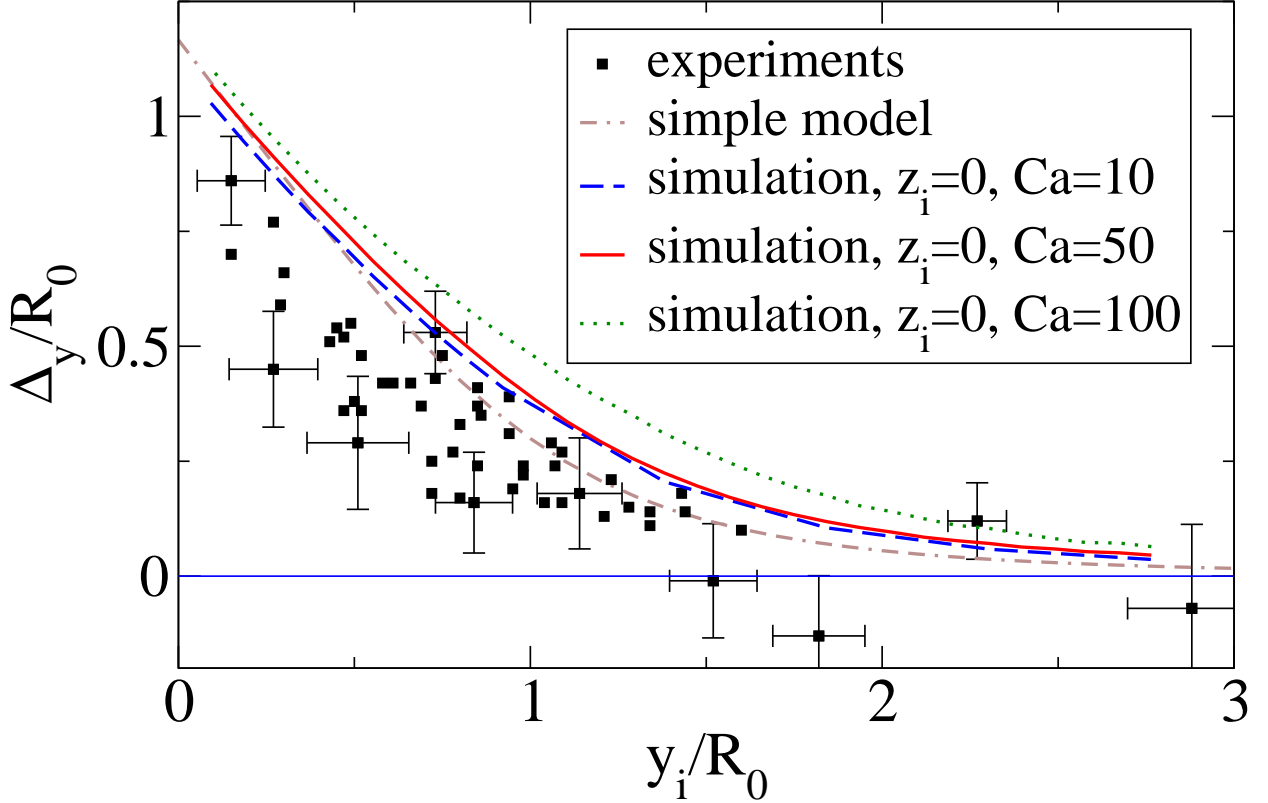


FIG. 6. Simulated displacements in the y direction for $z_i = 0$, $\lambda = 1$, $\nu = 0.95$ ($\nu_a = 0.91$), $Ca \in \{10, 50, 100\}$, and comparison with experimental data (same data as in Fig. 3). Error bars correspond to a spatial uncertainty of $1 \mu\text{m}$. Only part of them are presented for clarity. For comparison, we also plot the curve obtained through our simple model (Eq. 1) with $\xi = 8U$ given by the U value obtained from Olla's theory⁴⁷ for $\nu = 0.95$.

B. Departure from interaction of two identical vesicles in a shear plane of a simple shear flow

Influence of polydispersity

Regarding the influence of polydispersity, we computed several sets of interaction curves, with $Ca = 10$, first changing the radius ratio so that $R_2/R_1 \in \{0.9, 1.1\}$, and then both reduced volumes, so that $\nu_1 = \nu_2 \in \{0.8, 0.99\}$. We find relatively small effects, not sufficient to explain all the data scattering : for instance, for $y_i/R_0 = 0.5$, the maximal variation in Δ_y is 9%. Such a small effect was expected from the qualitative discussion presented in Sec. III.

Influence of z_i

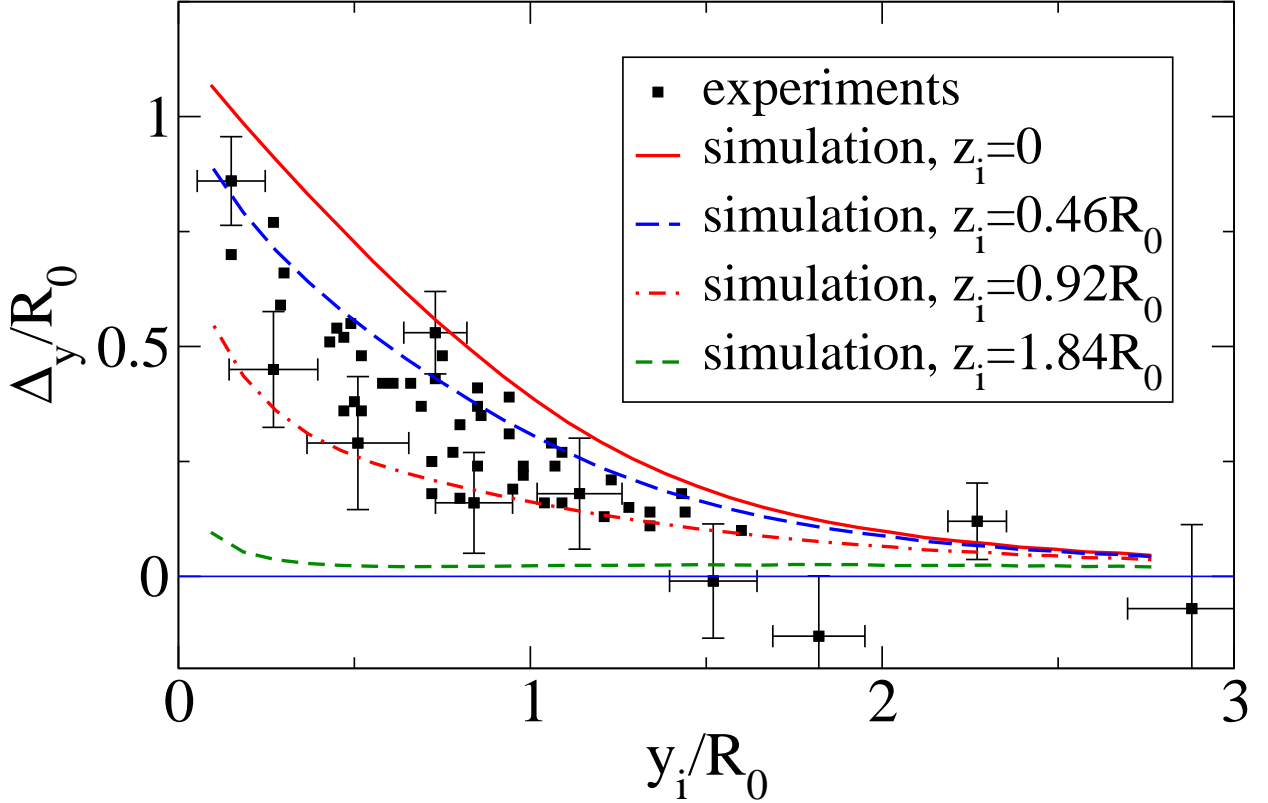


FIG. 7. Simulated displacements in the y direction for $z_i \in \{0, 0.46R_0, 0.92R_0, 1.84R_0\}$ ($0.92R_0 = a$), $\lambda = 1$, $\nu = 0.95$ ($\nu_a = 0.91$), $Ca = 50$, and comparison with experimental data (same data as in Fig. 3).

As expected, the deviation Δ_y decreases with z_i . Considering that the vesicles can be initially shifted in the vorticity direction by the maximal distance allowed by the focal depth of the microscope, a better agreement between experimental data and simulations is found (about 70% of experimental points, for vesicles of radii 10 μm).

Influence of the bottom channel wall

We consider now the influence of an imbalance between wall-outward migration and sedimentation. For simplicity and since gravity acts similarly on both vesicles, we only

consider the wall migration effect. As lift is a decreasing function of the distance to the wall⁴⁴, we expect the upper vesicle to migrate less relatively to the wall, so that the distance between the two vesicles is indirectly reduced due to that wall-induced lift forces.

We compare the whole trajectory obtained by our code with the one corresponding to the experiment shown on Fig. 2. The geometrical input parameters of the simulation are the reduced volume ν and the 3D effective radius a , in contrast with the experimentally measured reduced area ν_a and the 2D effective radius R_0 . From the study of isolated vesicles in simple shear flow, we find that, for $Ca = 10$, vesicles having same 2D cross-sections as the vesicles of Fig. 2 are characterized respectively by $\{\nu = 0.98, a = 8.9 \mu\text{m}\}$ and $\{\nu = 0.97, a = 8.6 \mu\text{m}\}$.

In order to quantify the bottom wall effect, we adopt the Green's function corresponding to a semi-infinite fluid^{52,53}, and include the quadratic part of the flow in the plane of shear, so that the imposed flow is $\dot{\gamma}y(1 - y/L_y)\mathbf{e}_x$. The initial distance of vesicle 1 from the wall is $y_{i,1} = 32 \mu\text{m}$. The comparison between the experiment and the numerical study is presented in Fig. 8, without and with wall, for vesicles in the same shear plane ($z_i = 0$). A possible shift $z_i/a = 0.39$ is also considered together with the presence of the wall.

As expected, lift by the wall leads to a slight initial attraction (a decrease of y for $x < 0$), which results in a slightly smaller final lateral displacement when $x \rightarrow \infty$. It appears however that this correction is too small to account for the remaining discrepancy between the simulations and the experiments, for which the initial attraction of around $1 \mu\text{m}$, that is seen on Fig. 2, appears on most trajectories.

Anyhow, this second-order effect is most probably linked with the presence of the wall, as suggested by recent simulations by Narsimhan et al., where interacting red blood cells in the vicinity of a wall are studied⁵⁴. They show that, for particles close enough to a wall, the relative lateral distance might decrease before interaction (see trajectories on their Fig. 15(b)), sometimes even leading to a completely different scenario of interaction involving swapping trajectories where particles do not cross. As shown by the authors, the presence of the bottom wall in the y direction induces the formation of a recirculation vortex behind the first particle, which is mainly responsible for the initial attraction. It is likely that when walls are also present in the z direction, as is the case in the experiment, the strength and extension of this recirculation are larger, leading to the stronger attraction observed in the first stage of experimental trajectories.

To sum it up, starting from comparable results for experiments and simulations, we

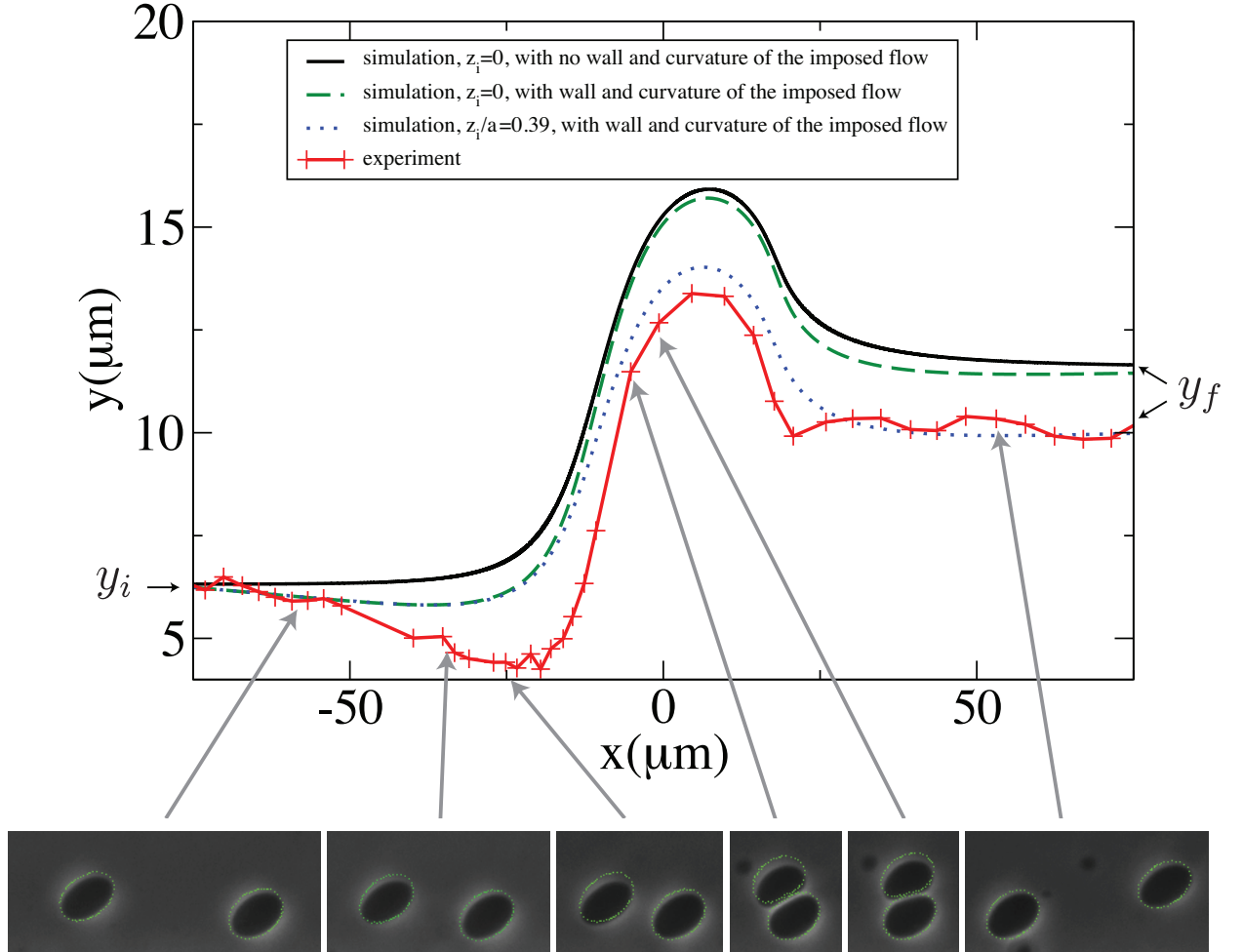


FIG. 8. Influence of the presence of the wall and the curvature of the imposed flow: comparison between the trajectory $y(x)$ of the experiment of Fig. 2 and the simulations, where we consider $Ca = 10$. For six selected relative positions x , the raw experimental pictures are shown, on which the simulated shapes are superimposed for the case where the influences of the wall and curvature of the imposed flow are considered, and $z_i/a = 0.39$ (dotted line).

have shown that a shift in the vorticity direction and the contribution of walls, both being inherent to the experiment, lead to a decrease of the repulsion, thus to some scattering in the experimental data, that all lie right below the ideal curve given by the simulations.

C. Deflection in the vorticity direction

As an extension to experimental results, the model also allows to investigate the effect of the interaction on the deflection Δ_z .

In Fig. 9, we present the interaction curves $\Delta_y(z_i)$ and $\Delta_z(z_i)$, for $y_i = 0.92R_0$, the other parameters remaining the same as previously.

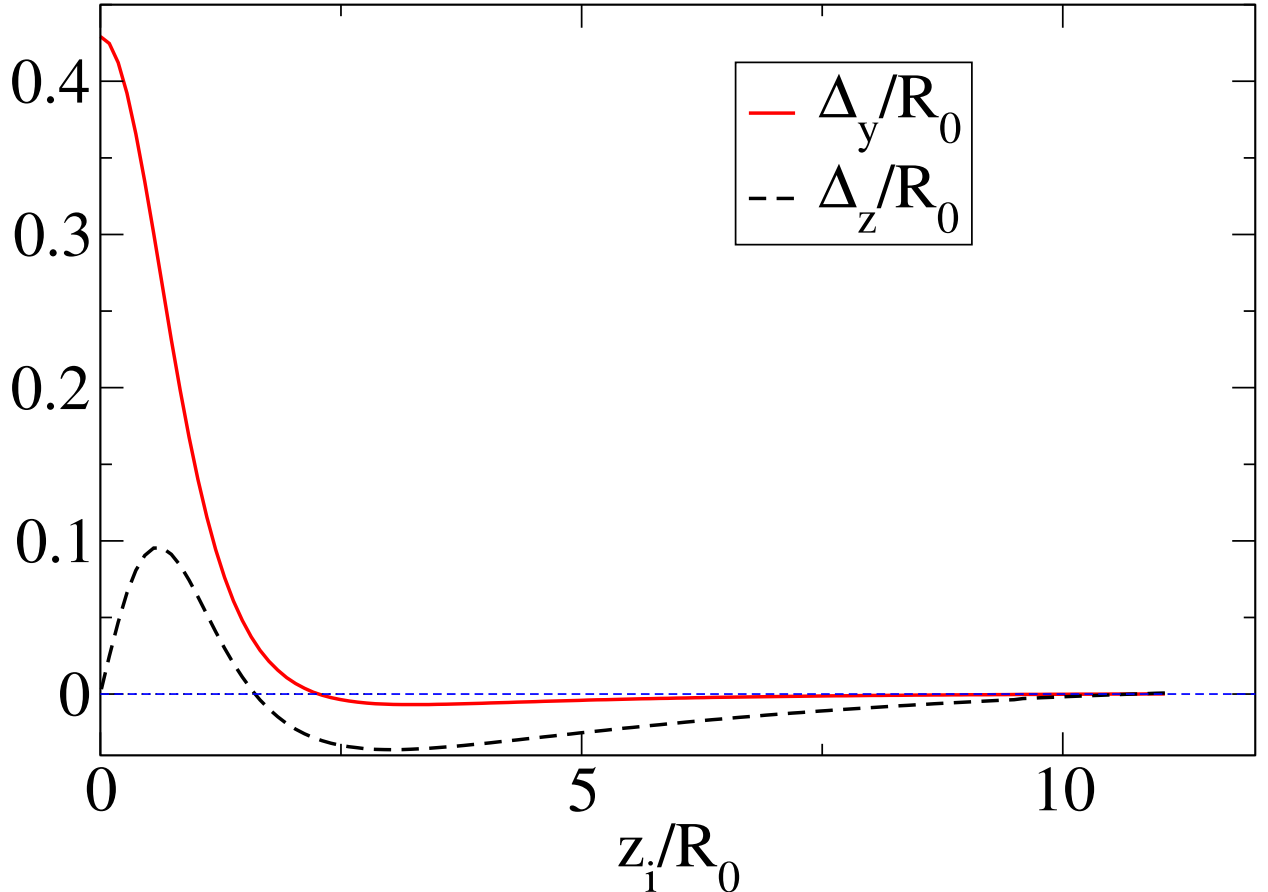


FIG. 9. Interaction curves for $\Delta_y(z_i/R_0)$ and $\Delta_z(z_i/R_0)$, for $y_i = 0.92R_0 = a$, $\lambda = 1$, $\nu = 0.95$, $Ca = 50$, and $|x_i| = |x_f| = 20a$

We find that there is a range of initial transverse positions for which the interaction leads to a transverse attraction between the vesicles, mostly in the vorticity direction. A similar phenomenon has been predicted for the interaction of capsules²², but not for drops¹⁷. An asymptotic study, for vesicles in the far field interacting regime, also predicts such an attraction³³. However, here the vesicles become close during the interaction, so a qualitative interpretation of the predicted attraction may involve the description of the flow of the thin

liquid film between the two tank-treading membranes, as done for drops¹⁷.

VI. HYDRODYNAMIC DIFFUSION

From the numerical study, one can expect to deduce results about the hydrodynamic diffusion properties of vesicle suspensions, in a regime where the solution is concentrated enough so that interaction effects are not negligible, but dilute enough so that pairwise interactions dominate over three-body interactions. We mostly study the case of self-diffusion, a phenomenon related to the average transverse motion of a single vesicle. We also find that an estimation of the collective diffusion coefficients is not possible only considering two-vesicle interactions, due to the long range of hydrodynamic interactions.

A. Self-diffusion

1. Theoretical background

We consider a homogeneous suspension of vesicles, described at a mesoscopic level by a volume fraction ϕ . For a given initial state, if this suspension is sheared by an imposed flow $\mathbf{v}^\infty = \dot{\gamma}y\mathbf{e}_x$, a given vesicle will interact with the others and, as a result, will undergo a net displacement \mathbf{X} from its original streamline. In an unstructured semi-dilute suspension, the transverse motion of the vesicle is expected to be a random walk due to successive interactions with different vesicles. At long times, its mean-squared displacement $\langle X_\alpha^2 \rangle$ is described by the self-diffusion coefficients $D_{s,\alpha}$, defined by

$$D_{s,\alpha} = \lim_{t \rightarrow \infty} \frac{1}{2} \frac{d\langle X_\alpha^2 \rangle}{dt},$$

with $\alpha \in \{y, z\}$, $\langle \cdot \rangle$ being an ensemble average over all possible initial states of the suspension¹⁷.

As detailed by Da Cunha and Hinch¹⁴, assuming that only two-vesicle interactions occur leads to the following expression for $D_{a,\alpha}$:

$$D_{s,\alpha} = \phi \dot{\gamma} a^2 f_\alpha, \tag{8}$$

with

$$f_\alpha = \frac{3}{2\pi} \int_{(y_i, z_i) \in [0, +\infty]^2} \Delta_{l,\alpha}^2 y_i dy_i dz_i, \quad (9)$$

where $\Delta_{l,\alpha}$ is the deviation of a test vesicle in the laboratory frame after one interaction. For identical vesicles, $\Delta_{l,\alpha} = \Delta_\alpha/2$. In the latter integral and from now on, all lengths are expressed in a units.

2. Analysis of the formal convergence of the diffusion coefficient

As the hydrodynamic interaction between two vesicles slowly decreases, the question of the convergence of the previous integral arises. As all displacements $\Delta_{l,\alpha}$ are bounded, the convergence of the expression 9 is linked to the contribution of the integration domain $\sqrt{y_i^2 + z_i^2} \gg 1$. We analyze this contribution by using an asymptotic study of two interacting quasi-spherical vesicles remaining very distant from each other, that was recently proposed by Gires *et al.*³³. We first need to determine the domain in the (y_i, z_i) space for which this asymptotic study is valid, a discussion that was not provided in the original paper. For the asymptotic study to be valid, vesicles must remain far enough along the whole trajectory, so that, at all times, $\|\mathbf{R}_{12}\| \gg 1$. As $\sqrt{y_i^2 + z_i^2} \gg 1$, one could expect this criterion to be always satisfied. However, let us consider $y_i = 0$. If there was no interaction, both vesicles would flow with the same velocity. But, since the velocity field induced by one vesicle is radial, vesicle collision may occur, which is inconsistent with the asymptotic approach. These considerations hint to the fact that the asymptotic study may not be valid for $y_i \ll 1$.

In order to get a more accurate validity criterion, we assume the asymptotic study to be valid for all times, and check that the inter-vesicle distance remains large. We expect that this approach can be used as each vesicle is not in the vicinity of a bifurcation phenomenon, such as the transition between the tank-treading and vacillating-breathing modes.

As detailed in Gires *et al.*³³, within this asymptotic approach with respect to the inter-vesicle distance, the trajectory of C_2 with respect to C_1 is of the form:

$$y(x) = y_i + \frac{1}{\dot{\gamma}} \left[\left(\frac{x^3}{(x^2+b^2)^{3/2}} + 1 \right) \frac{T_{xx}}{b^2} - \frac{2y_i T_{xy}}{(x^2+b^2)^{3/2}} + \left(\frac{(2x^2+3b^2)x}{(x^2+b^2)^{3/2}} + 2 \right) \frac{y_i^2 T_{yy}}{b^4} \right], \quad (10)$$

and

$$z(x) = \frac{(y(x) - y_i)z_i}{y_i} + z_i, \quad (11)$$

where $b = \sqrt{y_i^2 + z_i^2}$, and $\{T_{xx}, T_{xy}, T_{yy}\}$ are constants linked to the perturbation of the velocity field induced by the vesicles.

As the symmetry of the system does not depend on the reduced volume, we expect these scalings to be valid for vesicles of arbitrary deflation in the tank-treading regime, the dependency on the reduced volume being accounted for by the tensor $T_{\alpha\beta}$.

As $y(x) - y_i = O(b^{-2})$, the y distance between the vesicles will remain large if initially large. However, as $z(x) - z_i = z_i/y_i \times O(b^{-2})$, problems may arise at small y_i , as discussed earlier. In this case, the prevalent term in Eq. 10 is the term proportional to T_{xx}/b^2 . If $T_{xx} < 0$, this could lead to a minimal distance in the vorticity direction of the form $z_{\min} = z_i - c/(y_i z_i)$, with $c > 0$. In order that the asymptotic approach remains valid starting with $z_i \gg 1$, we impose the condition that $z_{\min} > z_i/d$, ($d > 1$), where d is a constant. This criterion can be achieved if $y_i > e/z_i^2$, with $e = dc/(d - 1) > 0$.

For initial positions satisfying this criterion, we find from Eqs. 10 and 11 that

$$\Delta_y = O\left(\frac{y_i^2 - z_i^2}{(y_i^2 + z_i^2)^2}\right), \quad (12)$$

$$\Delta_z = O\left(\Delta_y \frac{z_i}{y_i}\right). \quad (13)$$

It is clear from these expressions that the integral of Eq. 9, restricted to the region where the asymptotic expression is valid, is convergent.

As for the region of large z_i and small y_i with $y_i < e/z_i^2$, where the asymptotic expression is not valid, since $\Delta_{l,\alpha}^2$ is bounded by its maximal value and the integral of y_i on this region is finite, its contribution to the integral in Eq. 9 is bounded, and finally the whole integral is convergent.

3. Numerical determination of the self-diffusion coefficient

We now estimate the value of f_y (Eq. 9) that enters the expression of the diffusion coefficient (Eq. 8). For that purpose we need to run several simulations by starting with

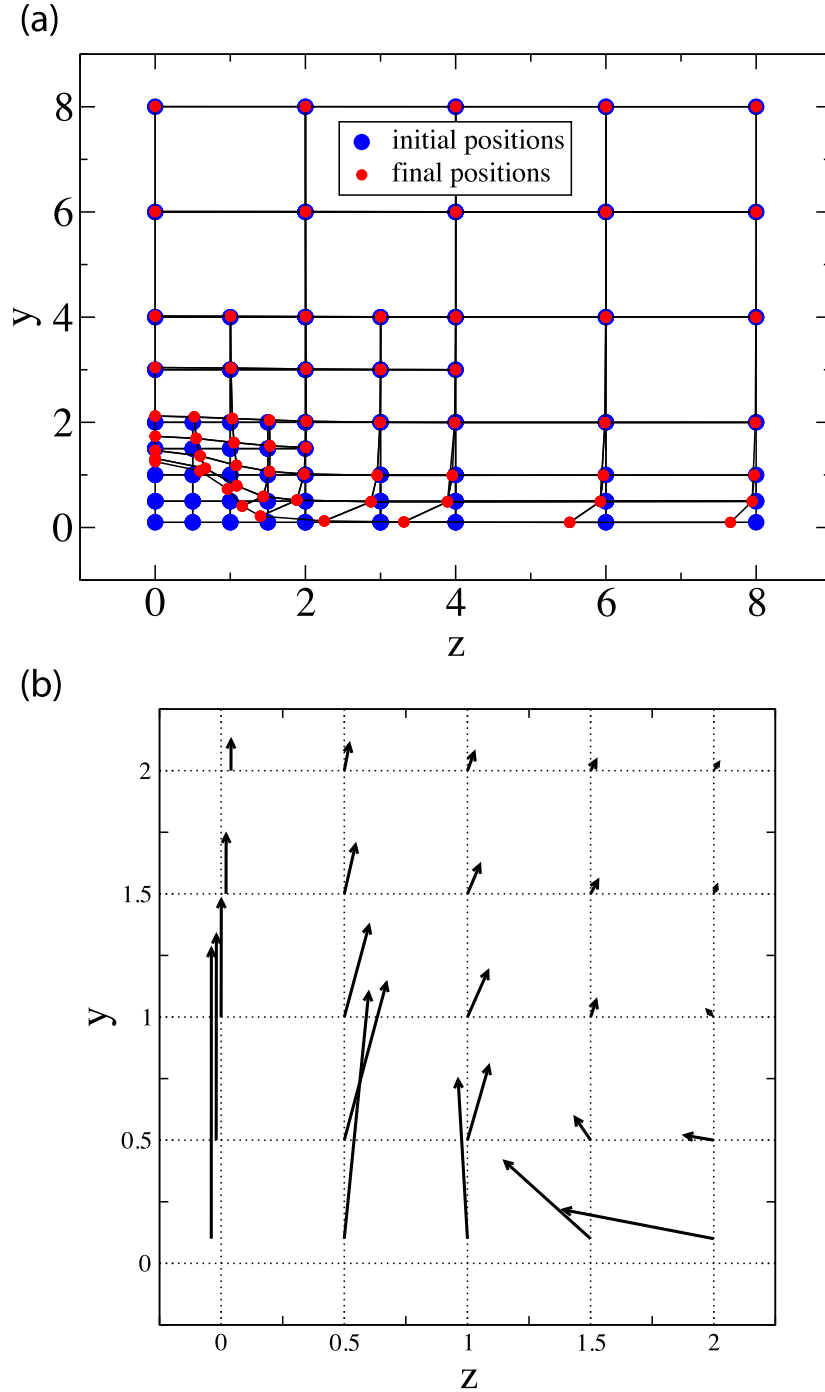


FIG. 10. (a) Evolution of the transverse position of a vesicle as a function of (y_i, z_i) . $\nu = 0.95$, $Ca = 50$. The lowest considered value for y_i is $y_i = 0.1a$, for which we chose $|x_i| = |x_f| = 80a$. For the other points, $|x_i| = |x_f| = 40a$. Panel (b) shows a zoom on the range $(y_i, z_i) \in [0, 2] \times [0, 2]$, where displacements are represented by arrows. For $z_i = 0$, arrows are slightly shifted to avoid superimposition.

	f_y	f_z
part A	0.028	0.002
part B	0.003	0.004
part C	0.001	0.005

TABLE II. Contributions of the sub-domains to the dimensionless self-diffusion coefficients f_y and f_z . $\nu = 0.95, Ca = 50$.

different initial position in the $y-z$ plane (which is the plane orthogonal to the flow direction) and determine by how much the initial relative positions y_i and z_i have varied (by amounts Δ_y and Δ_z) after the two vesicles have interacted. We discretize the domain of initial values (y_i, z_i) by considering the following domain size $[0, 8] \times [0, 8]$ (in units of vesicle radius a). The discretized lattice of initial positions is shown in Fig. 10(a) with dark gray disks (blue online). Since the interaction is important only when the two vesicles are separated by about 2 or 3 radii, the lattice has a wide enough periodicity far away from $(0, 0)$, whereas in the vicinity further refinements are chosen in order to gain numerical precision. More precisely, the domain is decomposed into three regions A , B and C , consisting in $[0, 2] \times [0, 2]$, $\{[0, 4] \times [0, 4]\} \setminus \{[0, 2] \times [0, 2]\}$ and $\{[0, 8] \times [0, 8]\} \setminus \{[0, 4] \times [0, 4]\}$. The lighter gray disks (red online) in Fig. 10(a) show the final relative positions y_f and z_f . We note that in region C the effect is weak, while it becomes more and more pronounced in region B and A. The contributions of the integral involved in Eq. 9 on the different sub-domains A , B and C are then evaluated using a trapezoidal rule. The results are given in Table II.

We find that the contributions for f_y are decreasing. As we proved the convergence of the expression, we expect the contributions of the remaining part of the plane to be at most of the order of the contribution of the sub-domain C, and thus get the following estimation for f_y :

$$f_y = 0.032 \pm 10\%. \quad (14)$$

The uncertainty of 10% is a rough estimate coming from a study of the sensitivity of the code to some numerical parameters, like a tension parameter used to preserve locally the area of the membrane.

For f_z , we do not get decreasing contributions, due to the slow decrease of Δ_z with z_i when $y_i \ll 1$. A similar study has been presented by Zhao and Shaqfeh³⁵, who calculated f_y for $\nu = 0.95$ and $Ca = 1$. Using the effective radius based on the surface as a length scale ($a' = \sqrt{S/4\pi}$, where S is the vesicle membrane area) they find $f_y = 0.028$. With the same convention instead of our choice of radius based on the volume, we find $f_y = 0.032\nu^{2/3} = 0.031$, for $\nu = 0.95$ and $Ca = 50$, which is a consistent result since lateral displacement increases with Ca (Fig. 4). Zhao and Shaqfeh also estimated the value of f_z , restricting to the integration domain $[0, 3] \times [0, 3]$: their value matches ours on the same region. However, the present study shows that restricting the integration to this domain is not sufficient to get a quantitative value of f_z , due to the slow decrease of the attraction with z_i for vesicles characterized by $y_i \ll 1$.

We are not aware of experimental measures of f_y to which we could compare our estimation. On the basis of studies on suspensions of spheres, the assumption of considering only two-vesicle interactions could be a good approximation up to volume fractions of about 10%⁵⁵.

4. Discussion

From simulated trajectories, Loewenberg and Hinch¹⁷ calculated f_y and f_z for pairs of drops as a function of viscosity ratio and capillary number. They evoke the scaling at long distance $\Delta_\alpha \sim 1/(y_i^2 + z_i^2)$, which is similar to ours, to prove the convergence of the integral of Eq. 9. It appears that in the case of drops, restricting the integration domain to A+B is sufficient, for f_y as for f_z . For $\lambda = 1$, f_y was found to be around 0.03 ± 0.01 , depending on the capillary number, a result close to ours. A more quantitative comparison is precluded by the dependency with capillary number and the difference in nature between the elastic restoring forces involved in drops and vesicles. Interestingly, Loewenberg and Hinch¹⁷ find $f_z \simeq 0.004$, while we already find a result 3 times larger by integration over A+B+C. We can conclude that anisotropy in self-diffusion is lower for vesicles than for drops. This weaker anisotropy is also stated by Lac and Barthès-Biesel in their study of capsules collisions, though f_y and f_z are not calculated²².

B. Down-gradient diffusion

The collective diffusion property of a vesicle suspension can be modeled in the following way: we consider a suspension of vesicles with a linearly increasing concentration given by $\phi = \phi_0 + \alpha y$, sheared by an imposed flow $\mathbf{v}^\infty = \dot{\gamma} y \mathbf{e}_y$. As a result of the hydrodynamic interactions between the vesicles, we expect a collective diffusion of the vesicles to appear, consisting of a transverse flux $\mathbf{j} = j \mathbf{e}_y$ of vesicles. As for molecular diffusion due to thermal motion, \mathbf{j} is expected to be in the opposite direction of $\nabla \phi$, of order $O(\alpha)$. Thus, for $\frac{\alpha a}{\phi_0} \ll 1$, we expect that $j = -D_{c,y} \alpha$, with $D_{c,y} > 0$. As done by Da Cunha and Hinch in the case of rough spheres¹⁴, we tried to estimate $D_{c,y}$ assuming only two-vesicle interactions. This leads to an expression involving the integral of $y_i^2 \Delta_y$ over the plane. However, as $\Delta_y = O(\frac{y_i^2 - z_i^2}{(y_i^2 + z_i^2)^2})$ and the integral of $\frac{y_i^2 (y_i^2 - z_i^2)}{(y_i^2 + z_i^2)^2}$ over $[0, y_0] \times [z_0, +\infty]$, with $(y_0, z_0) \in \mathbb{R}_+^{*2}$, is divergent, it turns out that the estimated expression is not convergent. A renormalization procedure, analogous to the one used by Batchelor^{1,56}, and followed by Wang *et al.*⁵⁷ in the case of the study of the hydrodynamic diffusion properties of a suspension of spheres, may lead to a convergent expression. It is hoped to investigate this matter further in a future work.

VII. CONCLUSION

We performed an experimental and numerical study of the trajectory deviations of identical vesicles interacting in shear flow. In experiments, restricted to pairs of vesicles in the same shear plane, the amplitude of the net displacement decreases quickly when the initial lateral distance increases and becomes negligible when this distance is larger than approximately two vesicle radii.

A simplified model based on the well established law for the lift of a vesicle near a wall was proposed, which allows to estimate quantitatively how the displacement should vary with the mechanical properties of the vesicles.

With no fitting parameter, the deviations are found to be in rather good agreement with our 3D simulations, even if smaller deviations are found experimentally. We found that the main part of this discrepancy can be due to differences between the experimental configuration and the ideal case of unbounded shear flow where the two vesicles would be perfectly coplanar. The effect of walls, recently highlighted by Narsimhan *et al.*⁵⁴, would

need to be quantified thoroughly in complementary experiments where our requirements of similar deflation within the pair of vesicles could be loosened for simplicity, since the effect of deflation has been characterized and shown to be weak. We also indicate that, according to partial results not shown here, the requirement of identical size within a pair may be released, as rescaling of the displacements by the average radius R_0 of two vesicles of different size lead to a similar curve for Δ_y/R_0 as a function of y_i/R_0 .

In addition, displacements in the vorticity direction were explored through the simulations and found to be about an order of magnitude lower than in the shear direction, with a range of initial distances leading to a weak attraction of vesicles.

Shear-induced diffusion coefficients can be obtained by a proper averaging of the net displacement over all initial configurations. The self-diffusion, related to the random walk of vesicles in a suspension, can be quantified using a discrete integration over a relatively small domain for the diffusivity in the shear direction, and could be determined in the vorticity direction if a larger integration area was considered, due to the slower decrease of the amplitude of displacement in that direction. Note that this integration would not have been possible in 2D⁵⁸ where the displacements would scale like $1/y$ instead of $1/y^2$.

An estimation of the down-gradient diffusivities as defined by Da Cunha and Hinch¹⁴ was not possible due to the long range of hydrodynamic interactions, leading to a divergence of the integrals. In this case, the dilute limit assumption breaks down and one can no longer consider only pair interactions as is the case for rough spheres with short range interactions¹⁴.

Appendix A: Local conservation of the area

We present in this appendix results about the local conservation of the area of a vesicle, during a typical trajectory. The parameters chosen were ($Ca = 50, \lambda = 1, \nu = 0.95, y_i = 0.5a, z_i = 0$). First, we plot in Fig. 11 the maximal relative variation of the area of the mesh faces, between two time steps, if they were advected by the full velocity field (in the simulation, the vertices are only advected by the normal component of the velocity field).

We find that this maximum can reach values higher than one. However, the proportion of faces corresponding to such values stays lower than 0.1%, as shown in Fig. 12.

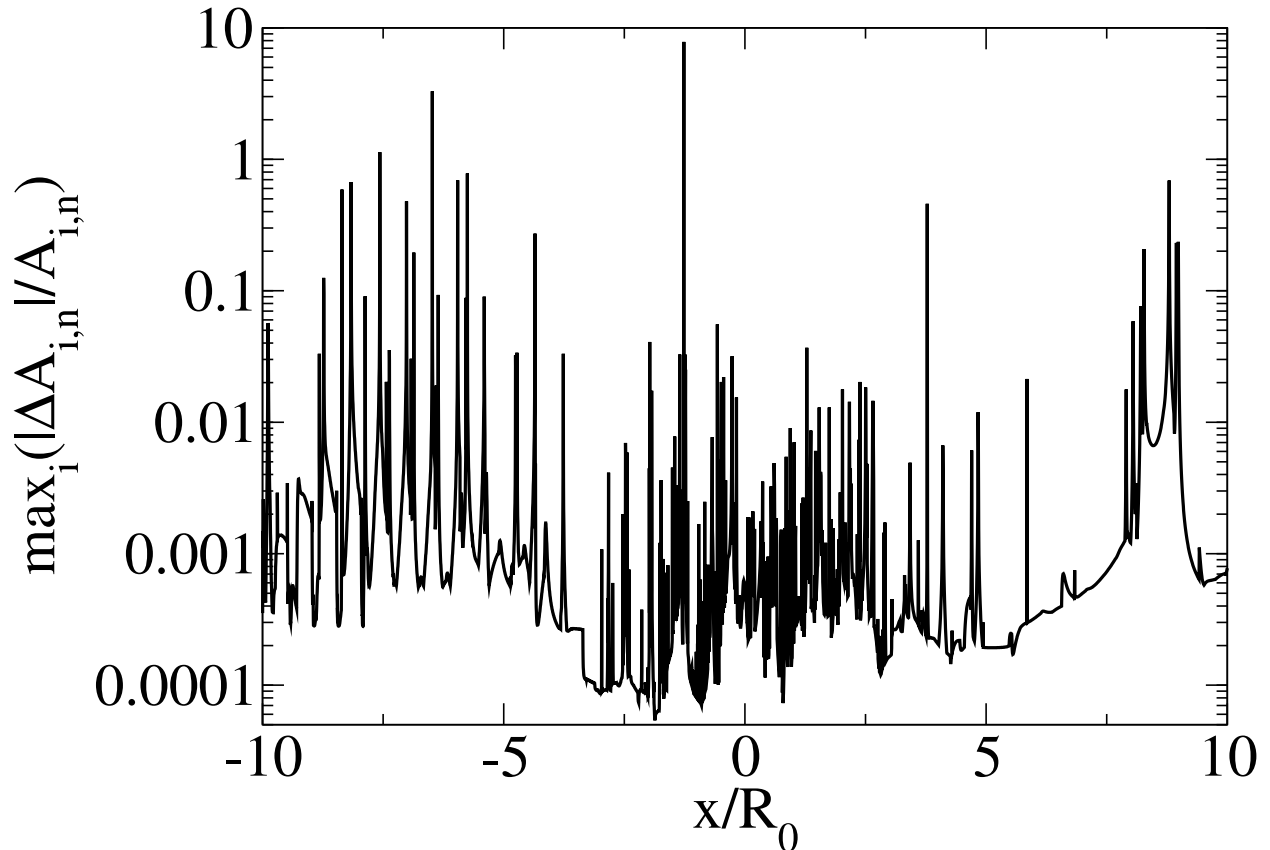


FIG. 11. Maximal relative variation of the area of the faces. $A_{i,n}$ is the area of face i at time step n , and $\Delta A_{i,n}$ is its variation during one time step, if it were advected by the full velocity field.

ACKNOWLEDGMENTS

The authors thank T. Biben (LPMCN, Lyon, France) for providing the initial simulation code and CNES (Centre National d'Etudes Spatiales) and ESA (European Space Agency) for financial support. P.-Y.G. also acknowledges funding from the French Ministry of Higher Education and Research, and the CNRS (Centre National de la Recherche Scientifique).

REFERENCES

- ¹G. Batchelor and J. Green, “The determination of the bulk stress in a suspension of spherical particles to order c^2 ,” *J. Fluid Mech.* **56**, 401–427 (1972).
- ²A. Z. Zinchenko, “Effect of hydrodynamic interactions between the particles on the rheological properties of dilute emulsions,” *J. Applied Math. Mech.* **48**, 198–206 (1984).

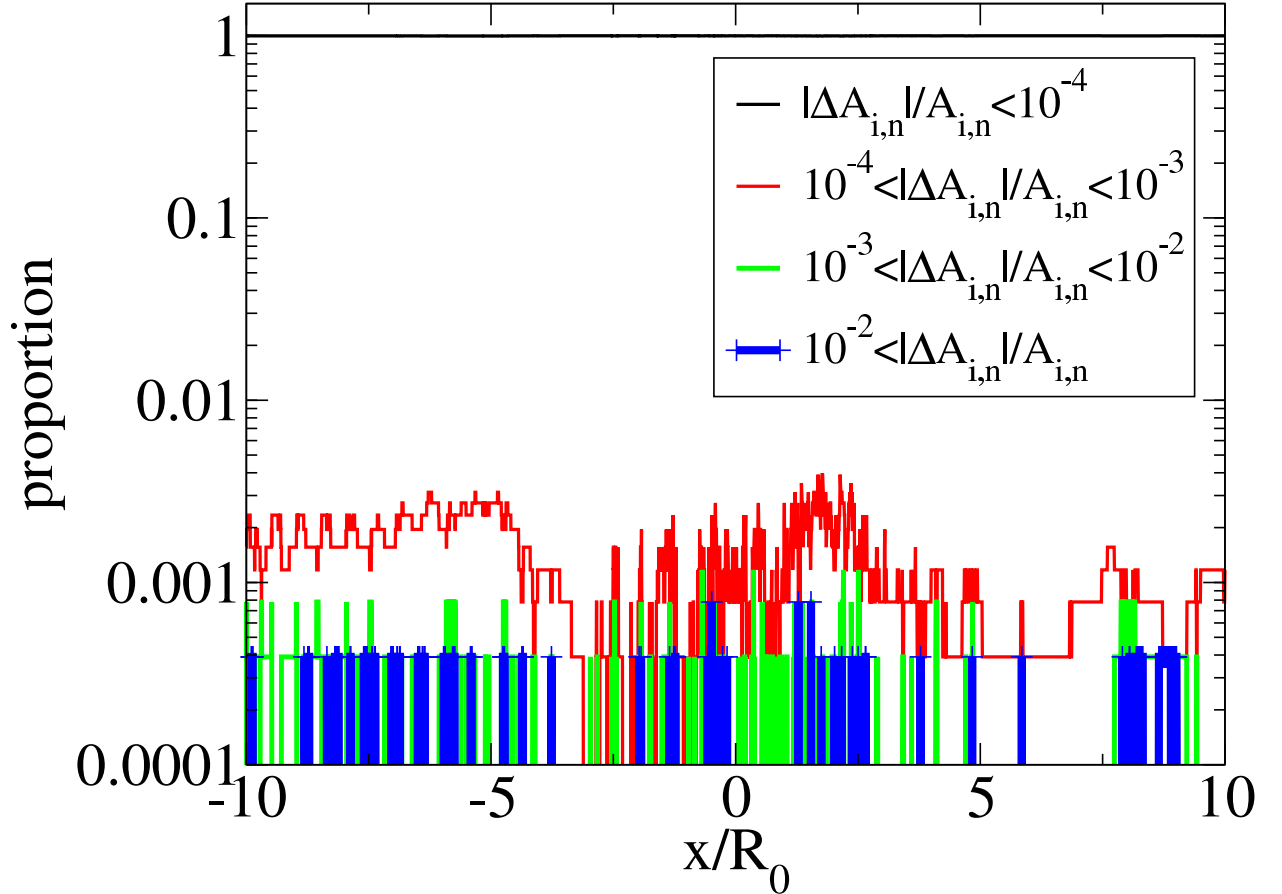


FIG. 12. Proportions of faces whose relative variation are in the ranges $[0, 10^{-4}]$, $[10^{-4}, 10^{-3}]$, $[10^{-3}, 10^{-2}]$ and $[10^{-2}, +\infty]$.

³H. L. Goldsmith, “Red cell motions and wall interactions in tube flow,” *Fed. Proc.* **30**, 1578 (1971).

⁴H. L. Goldsmith and J. C. Marlow, “Flow behaviour of erythrocytes,” *J. Colloid Interface Sci.* **71**, 383–407 (1979).

⁵W. Cha and R. L. Beissinger, “Evaluation of shear-induced particle diffusivity in red cell ghosts suspensions,” *Korean J. Chem. Eng.* **18**, 479 (2001).

⁶J. M. Higgins, D. T. Eddington, S. N. Bhatia, and L. Mahadevan, “Statistical dynamics of flowing red blood cells by morphological image processing,” *PLoS Computational Biology* **5**, e1000288 (2009).

⁷H. Zhao and E. S. G. Shaqfeh, “Shear-induced platelet margination in a microchannel,” *Phys. Rev. E* **83**, 061924 (2011).

- ⁸M. H.-Y. Tan, D.-V. Le, and K.-H. Chiam, “Hydrodynamic diffusion of a suspension of elastic capsules in bounded simple shear flow,” *Soft Matter* **8**, 2243–2251 (2012).
- ⁹S. D. Hudson, “Wall migration and shear-induced diffusion of fluid droplets in emulsions,” *Phys. Fluids* **15**, 1106–1113 (2003).
- ¹⁰R. Rusconi and H. A. Stone, “Shear-induced diffusion of platelike particles in microchannels,” *Phys. Rev. Lett.* **101**, 254502 (2008).
- ¹¹T. Podgorski, N. Callens, C. Minetti, G. Couplier, F. Dubois, and C. Misbah, “Dynamics of vesicle suspensions in shear flow between walls,” *Microgravity Sci. Technol.* **23**, 263–270 (2011).
- ¹²X. Grandchamp, G. Couplier, A. Srivastav, C. Minetti, and T. Podgorski, “Lift and down-gradient shear-induced diffusion in red blood cell suspensions,” *Phys. Rev. Lett.* **110**, 108101 (2013).
- ¹³F. P. Bretherton, “The motion of rigid particles in shear flow at low reynolds number,” *J. Fluid Mech.* **14**, 284–304 (1962).
- ¹⁴F. Da Cunha and E. Hinch, “Shear-induced dispersion in a dilute suspension of rough spheres,” *J. Fluid Mech.* **309**, 211–223 (1996).
- ¹⁵F. Blanc, F. Peters, and E. Lemaire, “Experimental signature of the pair trajectories of rough spheres in the shear-induced microstructure in noncolloidal suspensions,” *Phys. Rev. Lett.* **107**, 208302 (2011).
- ¹⁶L. Van Wijngaarden and D. J. Jeffrey, “Hydrodynamic interaction between gas bubbles in liquid,” *J. Fluid Mech.* **77**, 27– 44 (1976).
- ¹⁷M. Loewenberg and E. Hinch, “Collision of two deformable drops in shear flow,” *J. Fluid Mech.* **338**, 299 (1997).
- ¹⁸S. Guido and M. Simeone, “Binary collision of drops in simple shear flow by computer-assisted video optical microscopy,” *J. Fluid Mech.* **357**, 1–20 (1998).
- ¹⁹R. K. Singh and K. Sarkar, “Effects of viscosity ratio and three dimensional positioning on hydrodynamic interactions between two viscous drops in a shear flow at finite inertia,” *Phys. Fluids* **21**, 103303 (2009).
- ²⁰D.-V. Le and K.-H. Chiam, “Hydrodynamic interaction between two nonspherical capsules in shear flow,” *Phys. Rev. E* **84**, 056322 (2011).
- ²¹E. Lac, A. Morel, and D. Barthès-Biesel, “Hydrodynamic interaction between two identical capsules in simple shear flow,” *J. Fluid. Mech.* **573**, 149 (2007).

- ²²E. Lac and D. Barthès-Biesel, “Pairwise interaction of capsules in simple shear flow: three-dimensional effects,” *Phys. fluids* **20**, 040801 (2008).
- ²³P. Pranay, S. G. Anekal, J. P. Hernandez-Ortiz, and M. D. Graham, “Pair collisions of fluid-filled elastic capsules in shear flow: Effects of membrane properties and polymer additives,” *Phys. Fluids* **22** (2010).
- ²⁴T. Omori, T. Ishikawa, Y. Imai, and T. Yamaguchi, “Membrane tension of red blood cells pairwise interacting in simple shear flow,” *J. Biomech.* **46**, 548 (2013).
- ²⁵W. Helfrich, “Elastic Properties of Lipid Bilayers: Theory and Possible Experiments,” *Z. Naturforsch.* **28c**, 1–12 (1973).
- ²⁶J. Deschamps, V. Kantsler, and V. Steinberg, “Phase Diagram of Single Vesicle Dynamical States in Shear Flow,” *Phys. Rev. Lett.* **102** (2009).
- ²⁷A. Farutin, T. Biben, and C. Misbah, “Analytical progress in the theory of vesicles under linear flow,” *Phys. Rev. E* **81**, 061904 (2010).
- ²⁸T. Biben, A. Farutin, and C. Misbah, “Three-dimensional vesicles under shear flow: Numerical study of dynamics and phase diagram,” *Phys. Rev. E* **83**, 031921 (2011).
- ²⁹G. Danker and C. Misbah, “Rheology of a dilute suspension of vesicles,” *Phys. Rev. Lett.* **98**, 088104 (2007).
- ³⁰V. Kantsler, E. Segre, and V. Steinberg, “Dynamics of interacting vesicles and rheology of vesicle suspension in shear flow,” *Europhys. Lett.* **82**, 58005 (2008).
- ³¹V. Vitkova, M.-A. Mader, B. Polack, C. Misbah, and T. Podgorski, “Micro-macro link in rheology of erythrocyte and vesicle suspensions,” *Biophys. J.* **95**, 33 (2008).
- ³²M. Levant, J. Deschamps, E. Afik, and V. Steinberg, “Characteristic spatial scale of vesicle pair interactions in a plane linear flow,” *Phys. Rev. E* **85**, 056306 (2012).
- ³³P.-Y. Gires, G. Danker, and C. Misbah, “Hydrodynamic interactions between two vesicles in a linear shear flow: asymptotic study,” *Phys. Rev. E* **86**, 011408 (2012).
- ³⁴A. Farutin and C. Misbah, “Analytical and numerical study of three main migration laws for vesicles under flow,” *Phys. Rev. Lett.* **110**, 108104 (2013).
- ³⁵H. Zhao and E. S. G. Shaqfeh, “The dynamics of a non-dilute vesicle suspension in a simple shear flow,” *J. Fluid Mech.* **725**, 709–731 (2013).
- ³⁶V. Narsimhan, H. Zhao, and E. S. G. Shaqfeh, “Shear-induced particle migration and margination in a cellular suspension,” *Phys. Fluids* **24**, 011902 (2012).
- ³⁷A. Kumar and M. D. Graham, “Mechanism of margination in confined flows of blood and

- other multicomponent suspensions,” *Phys. Rev. Lett.* **109**, 108102 (2012).
- ³⁸D. A. Fedosov, J. Fornleitner, and G. Gompper, “Margination of white blood cells in microcapillary flow,” *Phys. Rev. Lett.* **108**, 028104 (2012).
- ³⁹H. L. Goldsmith and S. Spain, “Margination of leukocytes in blood flow through small tubes,” *Microvas. Res.* **27**, 204 – 222 (1984).
- ⁴⁰A. W. Tilles and E. C. Eckstein, “The near-wall excess of platelet-sized particles in blood flow: Its dependence on hematocrit and wall shear rate,” *Microvasc. Res.* **33**, 211 – 223 (1987).
- ⁴¹W. S. Uijttewaal, E. J. Nijhof, P. J. Bronkhorst, E. Den Hartog, and R. M. Heethaar, “Near-wall excess of platelets induced by lateral migration of erythrocytes in flowing blood,” *Am. J. Physiol. Heart Circ. Physiol.* **264**, H1239–H1244 (1993).
- ⁴²C. Yeh and E. Eckstein, “Transient lateral transport of platelet-sized particles in flowing blood suspensions,” *Biophys. J* **66**, 1706 – 1716 (1994).
- ⁴³M. I. Angelova, S. Soleau, P. Meleard, J. F. Faucon, and P. Bothorel, “Preparation of giant vesicles by external ac electric fields. kinetics and applications,” *Progr. Colloid. Polym. Sci* **89**, 127–131 (1992).
- ⁴⁴G. Couplier, B. Kaoui, T. Podgorski, and C. Misbah, “Noninertial lateral migration of vesicles in bounded Poiseuille flow,” *Phys. Fluids* **20**, 111702 (2008).
- ⁴⁵M. Abkarian, C. Lartigue, and A. Viallat, “Tank treading and unbinding of deformable vesicles in shear flow: Determination of the lift force,” *Phys. Rev. Lett.* **88**, 068103 (2002).
- ⁴⁶N. Callens, C. Minetti, G. Couplier, M. Mader, F. Dubois, C. Misbah, and T. Podgorski, “Hydrodynamic lift of vesicles under shear flow in microgravity,” *Europhys. Lett.* **83**, 24002 (2008).
- ⁴⁷P. Olla, “The lift on a tank-treading ellipsoidal cell in a shear flow,” *J. Phys. II France* **7**, 1533–1540 (1997).
- ⁴⁸S. Sukumaran and U. Seifert, “Influence of shear flow on vesicles near a wall: a numerical study,” *Phys. Rev. E* **64**, 011916 (2001).
- ⁴⁹P. M. Vlahovska and R. Serral Gracia, “Dynamics of a viscous vesicle in linear flows,” *Phys. Rev. E* **75**, 016313 (2007).
- ⁵⁰O. Zhong-can and W. Helfrich, “Bending energy of vesicle membranes : general expressions for the first, second and third variation of the shape energy and applications to spheres and cylinders,” *Phys. Rev. A* **39**, 1280 (1989).

- ⁵¹K. H. de Haas, C. Blom, D. van den Ende, M. H. G. Duits, B. Haveman, and J. Mellema, “Rheological behavior of a dispersion of small lipid bilayer vesicles,” *Langmuir* **13**, 6658 (1997).
- ⁵²C. Pozrikidis, *Boundary integral and singularity methods for linearized viscous flow* (Cambridge University Press, Cambridge, 1992).
- ⁵³B. Kaoui, G. Coupier, C. Misbah, and T. Podgorski, “Lateral migration of vesicles in microchannels: effects of walls and shear gradient,” *Houille Blanche* **5**, 112–119 (2009).
- ⁵⁴V. Narsimhan, H. Zhao, and E. S. G. Shaqfeh, “Coarse-grained theory to predict the concentration distribution of red blood cells in wall-bounded couette flow at zero reynolds number,” *Phys. Fluids* **25**, 061901 (2013).
- ⁵⁵R. Larson, *The structure and rheology of complex fluids* (Oxford University Press, Oxford, 1999).
- ⁵⁶G. Batchelor, “Sedimentation in a dilute suspension of spheres,” *J. Fluid Mech.* **52**, 245–268 (1972).
- ⁵⁷Y. Wang, R. Mauri, and A. Acrivos, “Transverse shear-induced gradient diffusion in a dilute suspension of spheres,” *J. Fluid Mech.* **357**, 279–287 (1998).
- ⁵⁸X. Li and C. Pozrikidis, “Wall-bounded shear flow and channel flow of suspensions of liquid drops,” *Int. J. Mult. Flow* **26**, 1247 (2000).